Demonstration of 8×10^{18} photons/second peaked at 1.8 Å in a relativistic Thomson scattering experiment

I. V. Pogorelsky,[1] I. Ben-Zvi,[1] T. Hirose,[2] S. Kashiwagi,[3] V. Yakimenko,[1] K. Kusche,[1] P. Siddons,[1] J. Skaritka,[1] T. Kumita,[2] A. Tsunemi,[4] T. Omori,[5] J. Urakawa,[5] M. Washio,[3] K. Yokoya,[5] T. Okugi,[5] Y. Liu,[6] P. He,[6] and D. Cline[6]

[1]*Accelerator Test Facility, Brookhaven National Laboratory, 820, Upton, New York 11973*

[2]*Department of Physics, Tokyo Metropolitan University, Hachioji-shi, Tokyo 192-0397, Japan*

[3]*Advanced Research Institute for Science and Engineering, Waseda University, Shinjuku-ku, Tokyo 169-8555, Japan*

[4]*Research and Development Center, Sumitomo Heavy Industries, Ltd., Tanashi-shi, Tokyo 188-8585, Japan*

[5]*KEK (High Energy Accelerator Research Organization, Tsukuba-shi, Ibaraki 305-0801, Japan*

[6]*Department of Physics and Astronomy, University of California, Los Angeles, California 90095*

(Received 7 February 2000; published 27 September 2000)

7.6×10^6 x-ray photons per 3.5 ps pulse are detected within a 1.8–2.3 Å spectral window during a proof-of-principle laser synchrotron source experiment. A 600 MW CO_2 laser interacted in a head-on collision with a 60 MeV, 140 A, 3.5 ps electron beam. Both beams were focused to a $\sigma = 32$ μm spot. Our next plan is to demonstrate 10^{10} x-ray photons per pulse using a CO_2 laser of $\sim$1 TW peak power.

PACS numbers: 41.60.Ap, 13.60.Fz, 41.75.Ht, 42.55.Lt

I. INTRODUCTION

The concept of an x-ray and gamma-ray laser synchrotron source (LSS) [1] based on Thomson scattering (or inverse Compton scattering) between laser photons and relativistic electrons is an example of the symbiotic relationship between accelerators and high-power lasers that may lead to novel femtosecond light-source facilities [2]. Enticed by these prospects, the Brookhaven Accelerator Test Facility (ATF) started proof-of-principle study of the LSS based on the combination of a photocathode rf linac and picosecond CO_2 laser [3,4]. Later, the study evolved into the Japan–U.S. Collaboration aimed to develop a polarized positron source for the Japan linear collider. This projected source will be based on $e^- e^+$ pair production using Thomson-scattered polarized gamma rays [5,6].

The experiment reported here is the first stage of developing the ultrahigh intensity LSS that combines a photocathode rf linac and a picosecond CO_2 laser. Selection of such components is based on a systematic approach to optimize the LSS towards maximum photon yield and positron production. Simultaneously, this approach opens the door to ultrahigh peak intensity femtosecond x-ray and gamma sources.

To compare with other previously demonstrated and proposed LSS (driven by ultrafast solid state lasers) [7–10], the CO_2 laser driver offers advantages reviewed in [3,4,11]. In particular, the CO_2 laser beam, having wavelength $\lambda = 10$ μm, carries 10 times more photons than a solid state laser ($\lambda = 1$ μm) of the same power. This implies a proportionally higher x ray yield for the LSS. Another advantage is the capability of gas laser technology for high repetition rate and high average power.

Two basic geometries are typically used in Thomson scattering: a 90° geometry where the e beam and laser beam are orthogonal to each other and a 180° geometry where they collide head-on with each other. In the 90° geometry the x-ray pulse length is defined not just by the laser but by the transverse time of the electron and laser focus that is about 300 fs at the typical rms beam size $\sigma \approx 50$ μm. In the 180° configuration, the x-ray pulse duration is defined primarily by the electron bunch length $\tau_x = \tau_b + \tau_L/4\gamma^2$, where τ_b is the electron bunch length, τ_L is the laser pulse length, and γ is the electron beam Lorentz factor. With the 200 fs electron bunches demonstrated from the rf linac [12] and the recent proposal on chirped bunch compression to 10–20 fs [13], the 180° geometry promises the absolute shortest x-ray pulses.

In designing a high-yield LSS, we choose backscattering (180°) also as the most efficient interaction geometry. The time interval when the counterpropagating focused laser and electron beams stay in interaction is normally $\pi r_L/\lambda$ times (where r_L is the laser beam radius) longer than in the 90° geometry, prompting correspondingly higher numbers of scattered photons. To obtain this ratio, we take a proportion between the Rayleigh range that defines the interaction length in the backscattering configuration to the laser beam radius that is important for the 90° configuration. Note that the 180° LSS is capable of producing femtosecond x-ray pulses using picosecond and even nanosecond laser pulses (for nanosecond pulses, channeling is required [14]).

In this paper, we describe results of the first proof-of-principle test of the CO_2 LSS on the picosecond time scale. We used the ATF 0.6 GW, 180 ps, linearly polarized CO_2 laser and the 3.5 ps, 0.5 nC, 60 MeV, low emittance $\varepsilon_n = 2$ mm mrad electron beam and demonstrated an x-ray yield of 2.8×10^7 photons/pulse, 8×10^{18} photons/sec, peaked at 1.8 Å.

II. DESCRIPTION OF THE EXPERIMENT AND RESULTS

The principle diagram of the CO_2 LSS experiment is shown in Fig. 1. The electron beam, produced by the

 © 2000 The American Physical Society

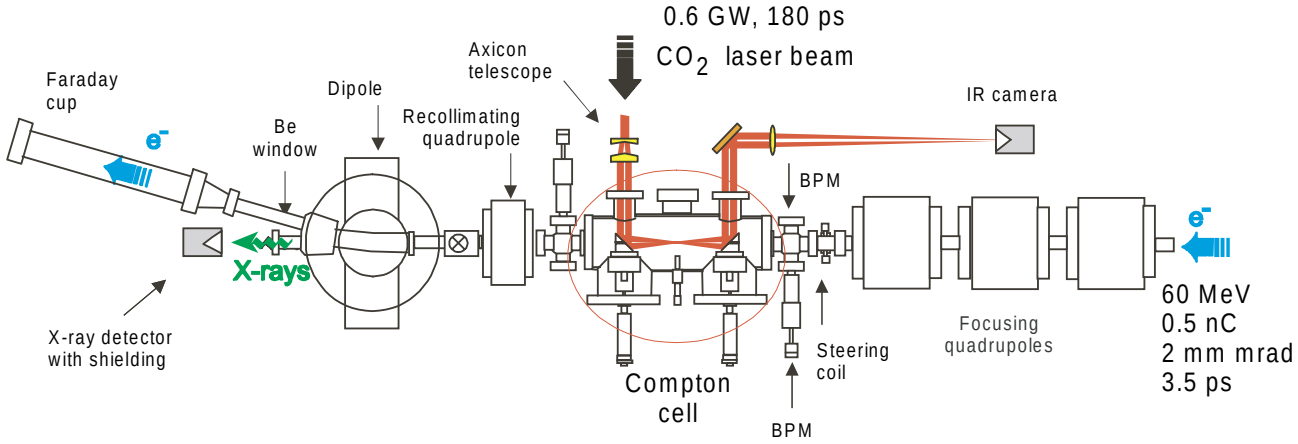

FIG. 1. (Color) Principle diagram of the CO_2 LSS experiment.

photocathode rf gun and accelerated to 60 MeV ($\gamma = 120$) in two linac sections, is focused in the middle of the Thomson interaction cell using upstream quadrupole magnets, as shown in the right-hand side of Fig. 1. Typical electron beam parameters in the interaction point are bunch charge 0.5–1.0 nC, energy spread 0.15%, normalized emittance $\varepsilon_n = 2$–4 mm mrad, bunch duration variable between 3.5–10 ps, and focus spot size down to $\sigma_b = 32$ μm. Steering coils allow transverse adjustment of the e-beam position inside the interaction cell. Recollimated after the interaction cell, the electron beam is deflected by the dipole magnet towards the beam stop equipped with a Faraday cup and radiation shield. Other e-beam diagnostics included strip line current monitors and phosphor beam profile monitors (BPM) positioned in several locations along the beam line. Detailed description of the high-brightness ATF linac, beam lines, and electron diagnostics can be found elsewhere [15,16].

The 0.6 GW, 180 ps pulses generated by the ATF CO_2 laser [17] are sent to a head-on collision (180° interaction geometry) with the e beam and focused into the same interaction point. In order to produce a tight focus of the CO_2 laser beam in this geometry, a short focal length optical element (in our case, a copper parabolic mirror with $F = 15$ cm) needs to be placed in the path of the e beam. Naturally, the mirror has a hole (5 mm in diameter) drilled along the e-beam axis. This hole serves to transmit the backscattered x rays as well. To avoid laser energy losses and material ablation at the hole edge, we telescope the initially quasi-Gaussian laser beam into an annular-shaped beam using a pair of ZnSe axicon lenses. Figure 2 shows a simulated profile of the axicon-transformed Gaussian beam. Antireflection coated ZnSe windows served to introduce the laser beam into the vacuum interaction cell and to extract the spent beam to diagnostics. A mirror mount remotely controlled with stepper motors permitted two-axis tilt of the focusing mirror for precision positioning of the laser focus at the interaction point. The spent laser beam has been extracted from the vacuum cell and recollimated onto an optical diagnostic using a similar parabolic mirror with a hole (see Fig. 1).

To ensure spatial overlap in the interaction point, both laser and electron beams were centered on the retractable 50 μm thick optical fiber crosshair. The position of the cross was precisely reproducible within the resolution of the visualization methods used (better than 10 μm). Cherenkov radiation from the fiber, reflected by the parabolic mirror and viewed by a high-magnification charge-coupled device (CCD) camera outside the cell, served to monitor the e-beam position.

The CCD camera was positioned in the path of the incoming CO_2 beam and could not be used *in situ* when the experiment was running and access to the e-beam line was prohibited. For remote verification of e-beam centering on the cross, we used auxiliary methods that included maximizing the bremsstrahlung signal by steering the e beam on the target cross and observing the cross shadow on the BPM immediately downstream from the interaction cell.

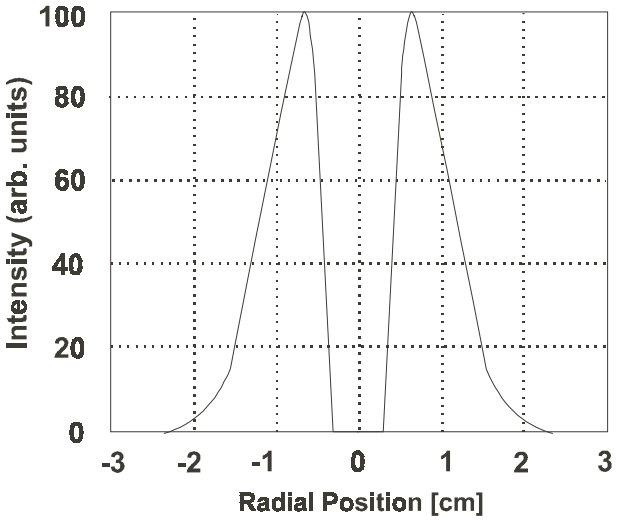

FIG. 2. Simulated annular-shaped radial distribution of the laser intensity after the axicon telescope.

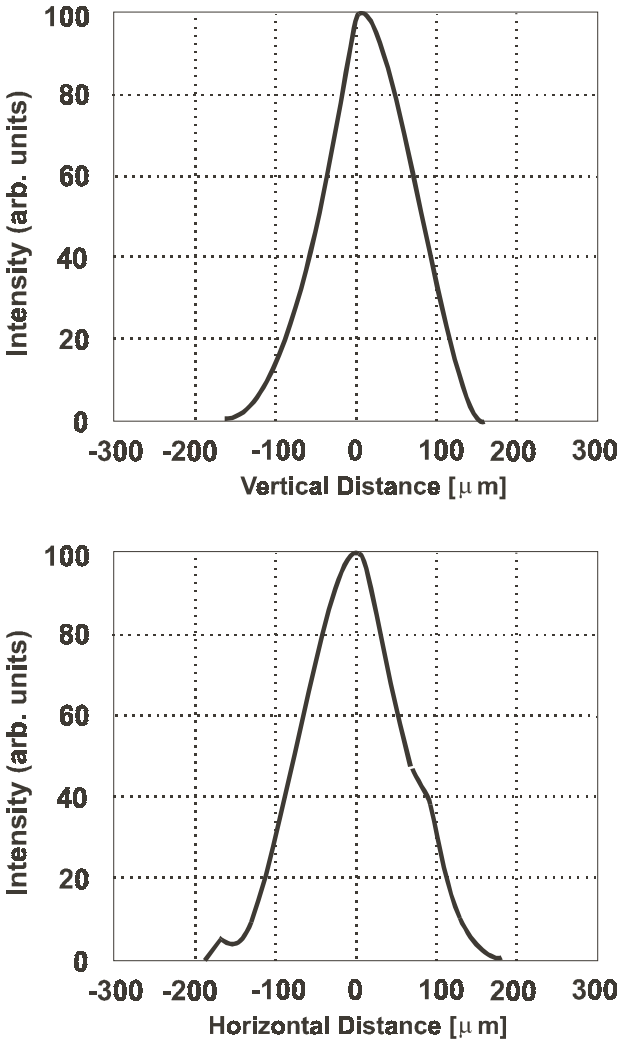

FIG. 3. Luminescence intensity profiles produced by the e beam on the phosphor screen.

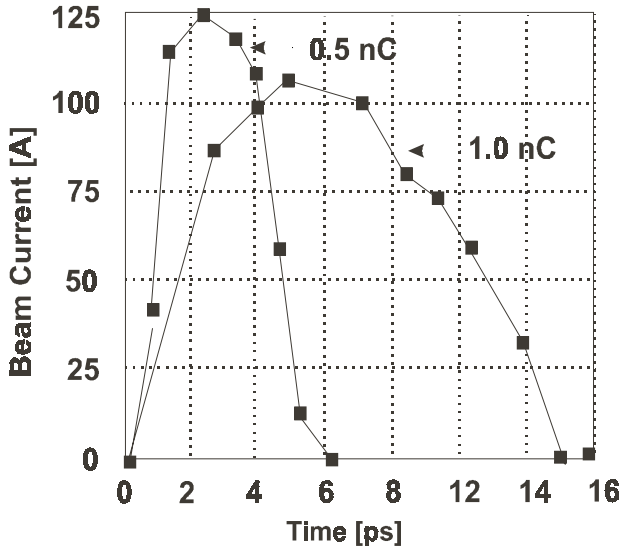

FIG. 5. Electron bunch longitudinal shape. The current is measured after the e-beam monochromator upon the rf phase tuning in the linac; 1 and 0.5 nC bunches were used, correspondingly, in the first and second experiment runs.

The phosphor screen, placed on the translation stage with the fiber cross, permitted observation of the e-beam spot size and intensity distribution with the same CCD camera that was used for the e-beam alignment on the cross. Figure 3 shows vertical and horizontal projections of the e-beam profile on the phosphor screen that give $\sigma_b \approx 50\ \mu$m. This value is close to the spatial resolution limit of the phosphor. To verify the e-beam size, we measured bremsstrahlung photons upon transverse scanning of the e beam with the 50 μm thick metal wire (see Fig. 4). Processing of the plot in Fig. 4 gives $\sigma_b = 32\ \mu$m.

We know that the temporal shape of the electron bunch normally defines the backscattered x-ray pulse. The bunch shape was measured by adjusting the rf phase in the

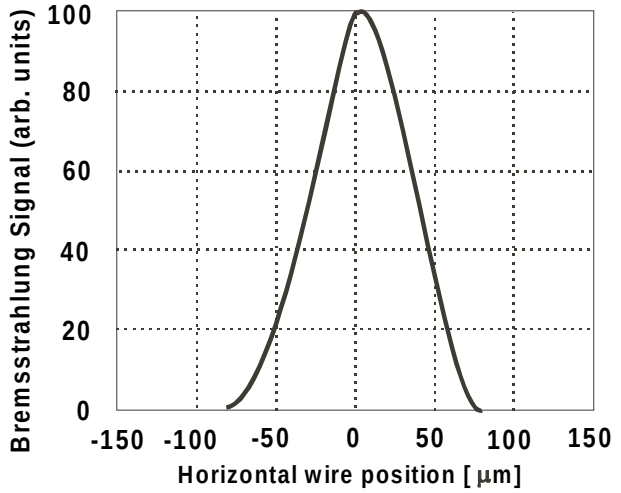

FIG. 4. Bremsstrahlung x-ray signal observed upon transverse scanning of the e beam with the 50 μm thick metal wire.

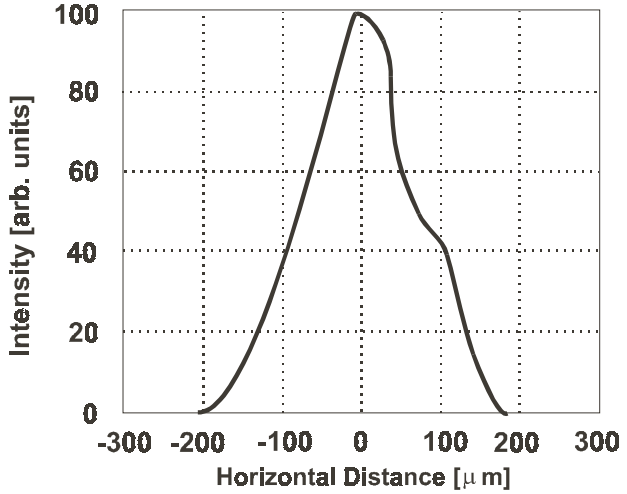

FIG. 6. Horizontal projection of the CO_2 laser focal intensity profile observed with the IR camera.

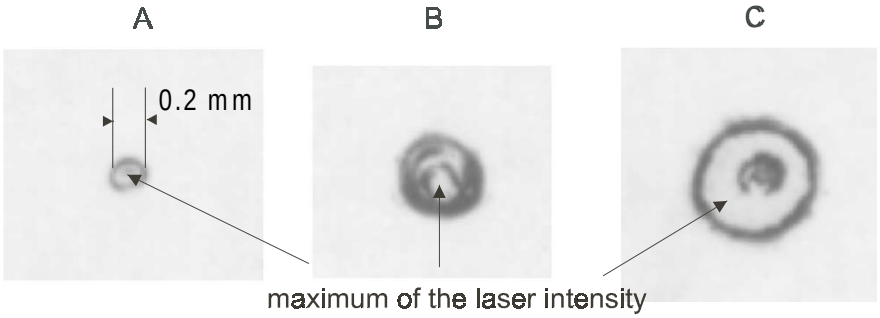

FIG. 7. Burn patterns made with the CO_2 laser beam on the thermal paper placed at the focal plane (image A) and at the distance 3.5 mm (image B) and 7 mm (image C) from the focus. Images are obtained at different attenuations of the laser beam. Marked white areas correspond to the strongest burn (white ash) surrounded by the areas of a less thermal exposure (black coal).

second linac section to produce a linear energy chirp to the electron bunch arriving at the monochromator positioned after the linac. A collimating slit in the dispersive region of the monochromator filters out a narrow slice of the bunch, which is then measured by a Faraday cup. The results of these measurements done for the first and second experiment runs, correspondingly 10 and 3.5 ps FWHM, are shown in Fig. 5.

Several methods used to assess the size of the laser beam in the interaction point included imaging of the focal area with a pyroelectric camera, transverse steering of the laser beam with the electron beam, and burn patterns on thermal paper.

The CO_2 laser focal spot in the interaction point imaged with 5× magnification on an Electrophysics 5400 pyroelectric video camera using a 75 cm focal length ZnSe lens is shown in Fig. 6. Based on these observations, the horizontal FWHM size of the laser spot is 170 μm (corresponds to $\sigma_L = 60$ μm in Gaussian approximation). However, caution shall be taken when using the magnified image for absolute measurements because of possible aberration in the imaging system. Because it is not very reliable for absolute measurement of the laser focal spot size, the magnified image is still an important tool for coalignment of the laser beam to the electron beam. We achieved this by adjusting the motor-mike-controlled focusing parabolic mirror so that the shadow of the inserted fiber cross is centered on the laser spot image.

Burn patterns on thermal paper provide a useful visualization of the laser beam evolution in the vicinity of the focus, as is shown in Fig. 7. However, this method cannot be used for absolute measurements of the laser spot size.

Plotting of the Thomson signal upon transverse scanning of the electron beam across the interaction region proved to be the most precise method to determine the laser spot size. Results shown in Fig. 8 indicate that the laser focus closely matches the electron beam size, $\sigma_b \approx \sigma_L \approx 32$ μm.

No transverse positioning jitter has been detected in either the laser or the electron beams within the resolution of our diagnostics (~10 μm). Laser alignment required correction only once a day. Focusing and positioning of the e beam required episodical correction due to linac phase drift.

A variable optical delay allows for adjustment of the timing between the electron bunch and the CO_2 laser pulse. Incidentally, this provides a tool to measure the CO_2 laser longitudinal profile. Figure 9 shows the observed dependence of the Thomson signal upon the delay time. Because the Thomson signal is linearly proportional to the laser intensity, we can use the obtained plots to characterize the time structure of the laser pulse. On the basis of these observations we conclude that the laser pulse is about 180 ps FWHM. The 600 MW peak power is obtained by time integrating the plot in Fig. 9 and normalizing it to the typical 200 mJ energy in the pulse.

The Thomson scattered x rays, diverging within a cone of $\theta = 1/\gamma = 8$ mrad, are detected with the 20 mm aperture Si diode placed outside the vacuum beam line 140 cm downstream from the interaction point (see Fig. 1). On the way to the detector, the x-ray beam passes through a

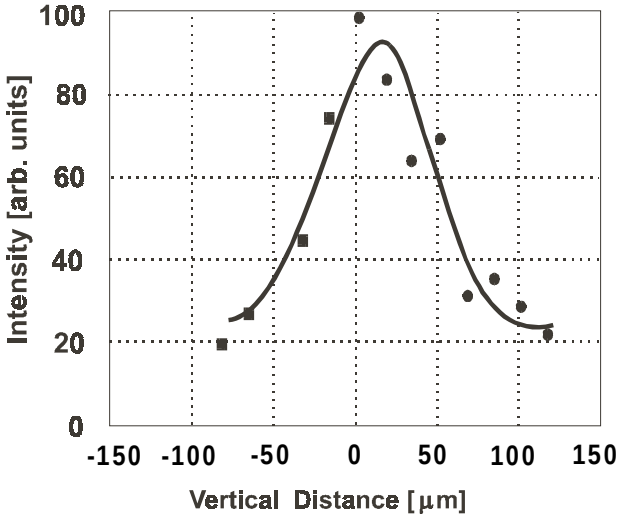

FIG. 8. Cross correlation of the electron and laser spot sizes when the Thomson scattering signal was measured during transverse scanning of the electron beam.

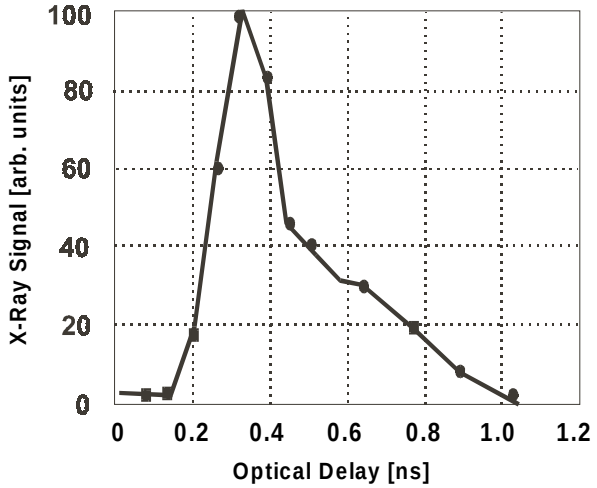

FIG. 9. Delay scan of the laser pulse.

5 mm hole in the focusing Cu mirror, propagates a total distance of 120 cm inside the vacuum beam line, exits through a 250 μm thick Be window, and propagates another 20 cm in the air. The electron beam is separated from the x rays by the bending dipole magnet and is sent to the beam stop. A lead hutch built around the detector was a sufficient screen from the background noise.

When the laser and electron beams are matched in focusing, alignment, and synchronization, we observe strong Thomson x-ray signals on the Si detector, much above the background level (defined by high energy x rays due to 60 MeV electron beam bremsstrahlung). The maximum measured signal was 2.2 V. A typical signal-to-noise ratio was up to 100 (see Fig. 10).

For the reported experiment conditions, the maximum scattered photon energy that results from the 0.117 eV CO_2 laser photon upshift by the 60 MeV electrons was 6.5 keV (1.8 Å). The minimum detected photon energy

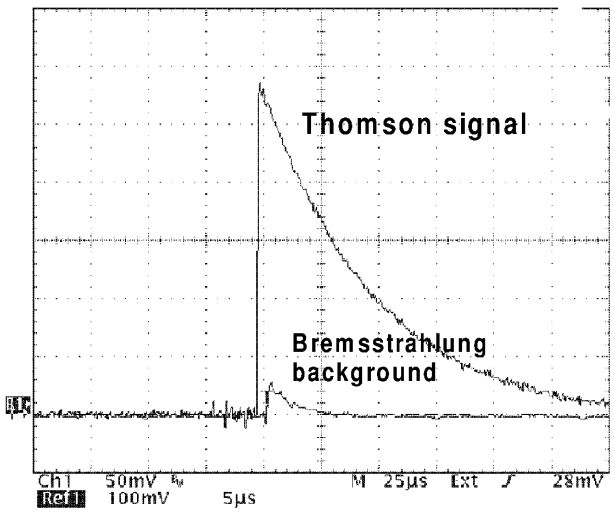

FIG. 10. Typical scope traces of the x-ray signal (at 100 mV/div) and noise (at 50 mV/div).

was 5 keV. This has been verified by placing spectrally selective Ti and Ni foil filters in front of the Si detector. The minimum energy threshold is due to the combined effect of the angular acceptance of the Si detector and x-ray absorption in the Be window and air.

III. DISCUSSION OF EXPERIMENTAL RESULTS AND SPECTRAL BRIGHTNESS

In order to measure the x-ray number based on the detector signal, the Si detector was calibrated based on the known average energy required to create the electron-hole pair in silicon (3.67 eV). For the measured diode circuit capacitance 330 pF, build up of the 2.2 V signal requires 730 pC charge accumulation. This charge is equivalent to 4.5 × 10^9 pairs and requires cumulative 1.7 × 10^{10} eV energy deposition to the Si. Dividing this by the average photon energy 5.85 keV, we obtain 2.9 × 10^6 photons deposited to Si. Based on the available data on transmission efficiency of the protective surface layer of the Si detector (80% averaged over 5.0–6.5 keV) and 95% photon absorption in the 250 μm thick Si slab, we calculate 3.9 × 10^6 photons reaching the detector.

Taking into account that an average spectral transmission of the beryllium and air in the 5–6.5 keV range is 48%, we estimate 7.6 × 10^6 photons in this spectral range before the Be window. Twenty-seven percent of the total photon number in the Thomson spectrum falls in the spectral range 5–6.5 keV. This leads to 2.8 × 10^7 photons/pulse produced via Thomson scattering at the laser electron interaction. This is about ten times higher in comparison with the number of the high-energy photons that actually contribute to the detector signal.

In the backscattering configuration, the x-ray pulse duration is equal to the electron bunch length (3.5 ps). This brings us to ~8 × 10^{18} photons/sec at the interaction region.

Next, we compare the measured photon flux with the theoretically expected value for the conditions of the BNL ATF LSS experiment. To calculate the expected number of Thomson scattered photons based on the laser and electron beam parameters we use the Monte Carlo code CAIN described in Ref. [18]. For a complete CAIN manual we refer to Ref. [19]. The input parameters for calculations are the laser wavelength, peak power, pulse duration and focal spot size, and the electron bunch energy, charge, length, emittance, and the focal spot size. The laser intensity distribution is assumed to be of Gaussian shape (transverse and longitudinal) and diffraction limited quality. In reality, the axicon telescope transforms the initially Gaussian beam described by equation

$$I_0(r) = \frac{P_0}{2\pi\sigma_0^2}\exp\left[-\frac{1}{2}\left(\frac{r}{\sigma_0}\right)^2\right] \qquad (1)$$

into the annular-shaped beam

$$I_0(r) = \frac{P_0}{2\pi\sigma_0^2}\left(1 - \frac{b}{r}\right)\exp\left[-\frac{1}{2}\left(\frac{r-b}{\sigma_0}\right)^2\right], \quad (2)$$

where P_0 is the laser power, σ_0 is the radius of the initial Gaussian beam, and $b = L\tan(\theta)$ is the inner radius of the annular, where L is the distance between two axicon lenses and θ is the refraction angle of the axicon. The intensity distribution described by Eq. (2) is shown in Fig. 2.

Solution of the Fresnel-Kirchhoff equations shows nearly identical intensity distribution at the focal plane for both laser profiles [see Figs. 11(a) and 11(b)]. This allows the use of the Gaussian beam approximation in the vicinity of the laser focus where the electron-laser interaction is the most efficient and the main part of the Thomson scattering flux is produced. At a longer distance from the focus, the difference between the Gaussian and annular beam becomes more pronounced. This is illustrated by Fig. 11(c). The assumption of the longitudinal Gaussian distributions as well as of the transverse electron beam distribution is even less critical and shall not affect the calculated integral number of scattered photons.

For the experimental conditions compiled in Table I, the CAIN code gives a total of 2.9×10^7 photons/pulse backscattered into the entire spectrum. This number closely matches the result derived above from the x-ray detector signal. To our knowledge, this is the highest photon yield ever demonstrated via laser Thomson scattering on relativistic electron beams.

An important characteristic of the LSS for potential applications is the spectral brightness. The backscattered photons are generated within a narrow cone with a solid angle $\Omega = 2\pi/\gamma^2$. Ideally, for every particular observation angle, the radiation spectrum is sharply peaked around its local frequency. The local peak frequency drops with an increase in the azimuthal angle ϕ, within the cone Ω, according to

$$\Delta\omega_x(\phi)/\omega_x^{\max} \approx \gamma^2\phi^2. \quad (3)$$

Note that only an infinitely long wave may be ideally monochromatic and well defined upon the scattering angle. In reality, the fractional bandwidth of the electron's radiation will depend upon the total number of laser wavelengths N measured over the electron-laser interaction distance

$$\Delta\omega_x'/\omega_x = 1/N\,. \quad (4)$$

Assuming that the effective interaction distance is equal to two laser Rayleigh lengths $2z_0$, where

$$z_0 = 4\pi\sigma_L^2/\lambda\,, \quad (5)$$

the time portion of the laser pulse that actually participates in the interaction with the electron bunch is $4z_0/c$. Taking the experimentally measured laser beam radius $\sigma_L = 32\ \mu$m, we obtain $z_0 = 1.25$ mm. Thus, $4z_0/c = 15$ ps, which comprises 500 laser wavelengths and results in $\Delta\omega_x'/\omega_x = 0.2\%$.

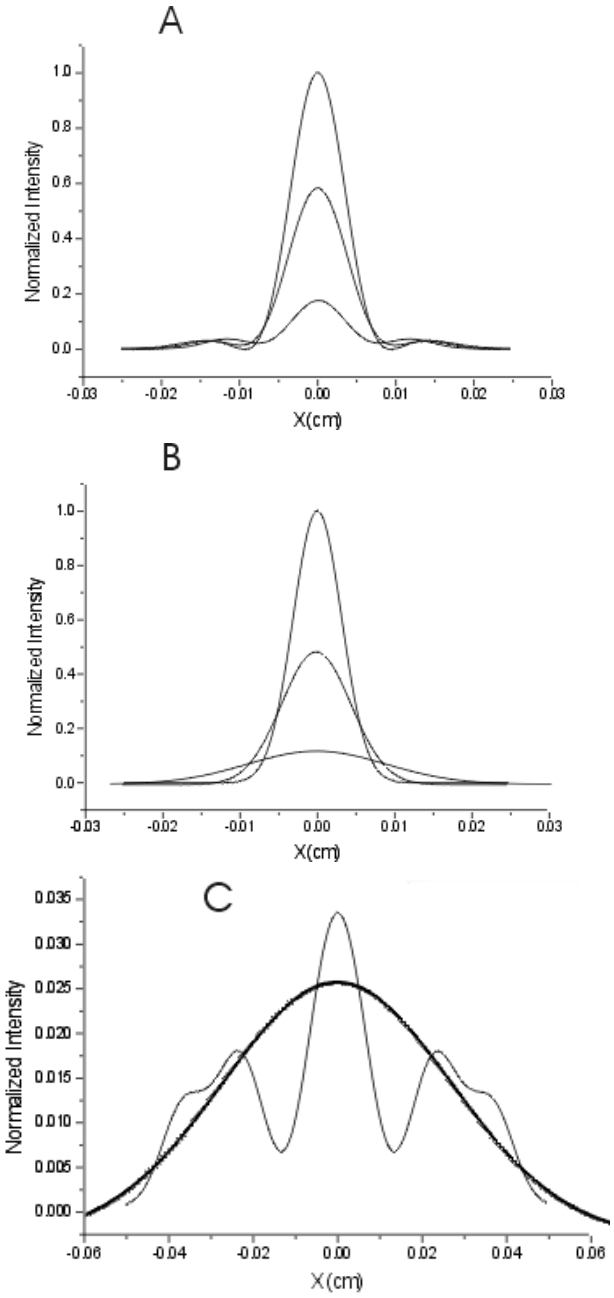

FIG. 11. Simulated transverse intensity distributions for annular-shaped and Gaussian CO_2 laser beams focused with the $F = 15$ cm lens: (a) annular-shaped beam at the focal plane ($\sigma = 32\ \mu$m) and at distances of 1.2 and 3.5 mm from the focal plane; (b) the same as in (a) but for the Gaussian laser beam; (c) comparison of the annular and Gaussian beams at the 7 mm distance from the focal plane.

It is also evident from the equation for the fundamental Thomson frequency, $\omega_x^{\max} = 4\gamma^2\omega$, that the bandwidth of the scattered x rays is directly related to the momentum spread or "temperature" of the e beam as

$$\Delta\omega_x''/\omega_x = 2\Delta\gamma/\gamma\,. \quad (6)$$

TABLE I. ATF CO_2 LSS experimental results and near-future design parameters.

Parameter	1st stage (1999)	2nd stage (2000)
CO_2 laser		
Pulse length (ps)	180	30
Pulse energy (J)	0.2	30
Peak power (GW)	0.6	1000
rms radius at focus (μm)	32	32
Waist length (mm)	2.5	2.5
Electron beam		
Electron energy (MeV)	60	60 (70)
Bunch duration FWHM (ps)	3.5	3.5
Bunch charge (nC)	0.5	0.5
Normalized emittance (mm mrad)	2	2
Momentum spread (%)	0.15	0.15
rms radius at focus (μm)	32	32
X rays		
Peak wavelength (Å)	1.8	2.6 (1.8)
Pulse duration (ps)	3.5	3.5
Photons per pulse (total spectrum)	2.9×10^7	1.3×10^{10}
Photons per sec (total spectrum)	8×10^{18}	4×10^{21}

For the ATF e beam, the temperature smearing in the x-ray spectrum is 0.3%.

The finite divergence of the electron beam at the interaction point also disperses the angular spectrum of the originated x rays. The e-beam divergence is equal to $\alpha = \sqrt{\varepsilon_n/\gamma\beta} = \varepsilon_n/\gamma\sigma_b$ and is approximately 0.5 mrad for the parameters of the present experiment. This results in 0.4% spectrum smearing,

$$\Delta\omega_x'''/\omega_x = (\varepsilon_n/\sigma_b)^2. \quad (7)$$

The combined minimum bandwidth

$$\Delta\omega_x/\omega_x = \sqrt{\Delta\omega_x'^2 + \Delta\omega_x''^2 + \Delta w_x'''^2}/\omega_x\,, \quad (8)$$

for the conditions of the ATF experiment, is equal to 0.5%. This narrow-bandwidth radiation is observed within the opening angle

$$\theta_i \approx (\Delta\omega_x/\omega_x^{\max})^{1/2}/\gamma\,. \quad (9)$$

For the ATF experiment, $\theta_I = 0.5$ mrad. The number of x rays radiated into this bandwidth is $N_{(\Delta\omega_x/\omega_x)} \approx (\Delta\omega_x/\omega_x)N_x$, where N_x is the total x-ray yield.

The aforementioned angular and spectral distributions of the backscattered radiation enter into the expression for brightness B, which is a cumulative characteristic of the radiation source

$$B = \frac{N_x\gamma^2}{4(\pi\sigma_b)^2\tau_b}\,, \quad (10)$$

equal to 2.8×10^{18} photons/sec mm^2 mrad^2 for the present ATF experiment conditions.

IV. CONCLUSIONS AND FUTURE PLANS

The reported experiment is the first step in the development of the high-brightness LSS at the ATF. The obtained agreement between theory and experiment allows straightforward extrapolation towards the next stage of the CO_2 LSS, which will utilize the 1000 times more powerful 1 TW, 30 ps CO_2 laser in the same interaction cell. With such a laser, the ATF will be ready to demonstrate LSS with the x-ray flux up to 4×10^{21} photons/sec (see the right-hand column in Table I).

We would like to conclude the discussion started in the Introduction on the advantages of the CO_2 laser driver for the femtosecond LSS, namely, spectral bandwidth and brightness.

Let us recall that the x-ray photon number per pulse $N_x \propto E_L Q\lambda/\sigma_L^2(1 + a^2/2)$, where E_L is the portion of the laser energy within the time interval $4z_0/c$ that actually participates in the interaction with the electron bunch and Q is the electron bunch charge. From the above expressions for N_x and B, we see that it is beneficial to choose values as high as possible for both parameters γ and λ. As long as $\lambda_x = \lambda(1 + a^2/2)/4\gamma^2$ is considered as an invariant, then choosing the CO_2 laser, with its wavelength ten times longer than the solid state laser wavelength, requires an electron beam a factor of $\sqrt{10}$ more energetic. This leads to an improvement of the angular divergence of the produced x rays [explaining a factor of γ^2 in Eq. (10)]. As mentioned previously, the backscattered x-ray intensity will also rise ten times proportionally to the photon number content per Joule of the laser energy. Combining these two factors together, we come to the conclusion that using a CO_2 laser as the LSS driver permits a 100 times increase in the LSS brightness compared with using a 1 μm laser of the same pulse energy.

We can foresee an argument that N_x and B can be increased due to the possibility of ~10 times tighter focusing of a short-wavelength laser. However, tighter laser focusing will require proportionally tighter focusing of the electron beam. Not talking about the problem of coalignment of such beams, we may start to see restrictions due to the space charge effect. In addition, for the tightly focused electron beam the x-ray bandwidth will be strongly dominated by the emittance-related component defined by Eq. (7).

In conclusion, we shall mention that the next stage of the ATF LSS experiment will open an opportunity for the study of Thomson harmonics using relativistic electron beams. With a 1 TW CO_2 laser beam focused into a $\sigma_L = 40$ μm spot, $I_0 = P_L/2\pi\sigma_L^2 = 10^{16}$ W/cm^2 laser intensity will be attained. According to the expression

$$a = 0.85 \times 10^{-9}\lambda\ [\mu\text{m}]I^{1/2}\ [\text{W/cm}^2],$$

this intensity corresponds to a normalized laser strength of $a \approx 1$, and the nonlinear Thomson scattering effect comes into view.

ACKNOWLEDGMENTS

We wish to thank all collaborators on the U.S.–Japan Compton experiment who contributed at different stages of the experiment preparation and, in particular, K. Dobashi, T. Muto, T. Kobuki, R. Kuroda, and Z. Segalov, the Optoel Company for designing the interaction cell to our specifications, W. Kimura and K. McDonald for providing essential optical components and diagnostics, R. Tatchyn for useful discussions, and R. Harrington for technical assistance. This study is supported by the U.S. Department of Energy under Contract No. DE-AC02-98CH10886 and Japan/U.S. cooperation in the field of High Energy Physics.

[1] P. Sprangle, A. Ting, E. Esarey, and A. Fisher, J. Appl. Phys. **72**, 5032 (1992).

[2] Recommendations of Basic Energy Sciences Advisory Committee Panel on Novel Coherent Light Sources, http://www.sc.doe.gov/production/bes/BESAC/ncls_rep.PDF

[3] I. V. Pogorelsky, BNL Report No. BNL-62447, 1995.

[4] I. V. Pogorelsky and I. Ben-Zvi, in *Proceedings of the Particle Accelerator Conference, Vancouver, Canada, 1997* (IEEE, Piscataway, NJ, 1998), p. 645

[5] T. Hirose, in *Proceedings of the International Workshop on Physics and Experiments with Linear Colliders, Morioka Iwate, Japan, 1995* (World Scientific, Singapore, 1996), p. 748.

[6] T. Okugi, Y. Kurihara, M. Chiba, A. Endo, R. Hamatsu, T. Hirose, T. Kumita, T. Omori, Y. Takeuchi, and M. Yosioka, Jpn. J. Appl. Phys. **35**, 3677 (1996).

[7] A. Ting, R. Fischer, A. Fisher, C. I. Moore, B. Hafizi, R. Elton, K. Krushelnick, R. Burris, S. Jadel, K. Evans, J. N. Weaver, P. Sprangle, M. Baine, and S. Ride, Nucl. Instrum. Methods Phys. Res., Sect. A **375**, 68 (1996).

[8] R. W. Schoenlein, W. P. Leemans, A. H. Chin, P. Volbeyn, T. E. Glover, P. Balling, M. Zolotarev, K.-J. Kim, S. Chattopadhyay, and C. V. Shank, Science **274**, 236 (1996).

[9] K. Nakajima, in *Proceedings of LASERS'97, New Orleans, Louisiana, 1997* (STS Press, McLean, VA, 1998), p. 778.

[10] T. Cowan, Nucl. Instrum. Methods Phys. Res., Sect. A (to be published).

[11] I. V. Pogorelsky, Nucl. Instrum. Methods Phys. Res., Sect. A **411**, 172 (1998).

[12] M. Uesaka, K. Kinoshita, T. Watanabe, T. Ueda, K. Yoshii, H. Harano, J. Sugahara, K. Nakajima, A. Ogata, F. Sakai, H. Dewa, M. Kando, H. Kotaki, and S. Kondo, in *Advanced Accelerator Concepts: Eighth Workshop*, edited by Wes Lawson, AIP Conf. Proc. No. 472 (AIP, New York, 1999), p. 908.

[13] X. J. Wang, in *Proceedings of the 1999 Particle Accelerator Conference (PAC99), New York* (IEEE, Piscataway, NJ, 1999), p. 229.

[14] I. V. Pogorelsky, I. Ben-Zvi, X. J. Wang, and T. Hirose, Nucl. Instrum. Methods Phys. Res., Sect. A (to be published).

[15] http://www.nsls.bnl.gov/AccTest/Beam_Lines/ATF_Beam_Lines.htm

[16] X. J. Wang, M. Babzien, K. Batchelor, I. Ben-Zvi, R. Malone, I. V. Pogorelsky, X. Qui, J. Sheehan, J. Skaritka, and T. Srinivasan-Rao, Nucl. Instrum. Methods Phys. Res., Sect. A **375**, 82 (1996).

[17] I. V. Pogorelsky, J. Fischer, K. P. Kusche, M. Babzien, N. A. Kurnit, I. J. Bigio, R. F. Harrison, and T. Shimada, IEEE J. Quantum Electron. **31**, 556 (1995).

[18] P. Chen, G. Horton-Smith, T. Ohgaki, A. W. Weidemann, and K. Yokoya, Nucl. Instrum. Methods Phys. Res., Sect. A **355**, 107 (1995).

[19] K. Yokoya, in Proceedings of the 7th International Workshop on Linear Colliders, Zvenigorod, Russia, 1997 (unpublished).

[20] E. Esarey, S. K. Ride, and P. Sprangle, Phys. Rev. E **48**, 3003 (1993).